Scalar mixing in bubbly flows: Experimental investigation and diffusivity modelling

E Alméras, F Euzenat, C Plais, F Augier, Frederic Risso, Véronique Roig

Scalar Mixing in Bubbly Flows: Experimental Investigation and Diffusivity Modelling

E.Alméras[1,2], F.Euzenat[1], C.Plais[1], F.Augier[1,*], F. Risso[2], V.Roig[2]

[1]IFP Energies nouvelles, Rond-point de l'échangeur de Solaize, BP 3, 69360 Solaize, France
[2]IMFT, Université de Toulouse and CNRS, Allée C. Soula, 31400 Toulouse, France
*Corresponding author (frederic.augier@ifpen.fr).

Abstract

Transport properties of scalars, as concentrations of a solute or temperature, are important for scale-up and design of operation units. An appropriate description of convective and diffusive mechanisms is required to predict local concentrations in complex geometries. In the case of gas-liquid bubbly flows, which are present in many chemical– or bio– reactors, effective diffusivity of scalars results from three contributions: molecular diffusion, Shear-Induced Turbulence (S.I.T.), i.e. turbulence induced by gradients of velocity in the continuous phase, and Bubble-Induced Turbulence (B.I.T.), i.e. turbulence generated by interactions of bubble wakes. In a previous work (Alméras et al., 2014, 2015), the diffusion resulting from B.I.T. has been characterized. Based on experiments performed in a homogeneous bubble column, it was shown that the transport can be modelled by an effective diffusion and a physical modelling has been proposed to predict the diffusion induced by B.I.T when other contributions are negligible.

In the present work, we have investigated the transport of a passive scalar in a complex bubbly flow at moderate gas volume fraction ($\alpha_g \leq 3\%$), involving a large-scale flow recirculation responsible for the development of shear-induced turbulence. Experimental mixing times measured by image processing in various operating conditions have been compared to numerical simulations of scalar transport. Simulations have been performed by means of an Eulerian RANS CFD model wherein the diffusion generated by B.I.T modelled by Alméras et al. 2015 is implemented in addition to the diffusion resulting from the S.I.T.

Results show that the diffusion caused by B.I.T. plays a major role in the mixing of scalars in the investigated flows. Neglecting this contribution leads to an important overestimation of the mixing time unless assigning arbitrary low values to the turbulent Schmidt number Sc_t (< 0.3) adapted a posteriori to the simulated cases. On the other hand, considering the scalar diffusivity by B.I.T leads to a good agreement between experiments and CFD simulations, with keeping the Schmidt number in the usual range adopted for mixing in S.I.T. [0.7-1]. The model is generic enough to reproduce the scalar transport for various gas injections, without any further user adaptation.

Keywords Bubbly flows, gas-liquid, scalar diffusivity, mixing, CFD, experiment

Research Highlights

- Diffusion coefficient of a scalar in bubbly flows
- Mixing by bubble-induced turbulence
- Effective diffusivity implemented in a two-fluid model.
- Validation by comparison between Experiments and CFD results

1. Introduction

Bubbly flows are very common in many industrial fields such as biology, chemistry, refining, and water treatment. They can be implemented in various contacting apparatus as aerated stirred reactors, bubble columns, air-lift columns (Laurent and Charpentier, 1974). Resulting hydrodynamics is generally complex due to the presence of different sources of agitation as macro-scale recirculation, buoyancy-driven instabilities, turbulence and relative motion between phases. Depending on the technology and the geometry of contactors, overall hydrodynamics responsible for concentration transport skip from quasi-plug flow to well stirred flow (Deckwer, 1992). The prediction of global hydrodynamics is a major issue for process design as it strongly impacts performances of considered gas-liquid contacting units.

In this goal, as an alternative to expensive experimental studies, Computational Fluid Dynamics (CFD) is a very powerful tool for prediction of global and local hydrodynamics. It has been applied for decades to gas-liquid flow characterization (Delnoij et al., 1997; Rafique et al., 2004) and nowadays, different types of models exist to simulate bubbly flows. For example, interface reconstruction models such as Volume Of Fluid models (VOF) allow to predict the bubble size and shape (Li et al., 2000; Dai et al., 2004) while Lagrangian models can calculate individual bubble trajectories (Lau et al., 2014). But these two families of models are still unable to predict dense bubbly flows at large industrial scales because the calculation of each bubble position and/or shape is too-much CPU-time consuming and that bubbles interactions are difficult to reproduce. Large geometries involving bubbly flows are often simulated by using the so-called two-fluid models (Jakobsen et al., 2005). The formalism of two-fluid models is based on phase-volume and time averaging. As a consequence, mean phase velocity and fraction fields are solved. The two phases are considered as two interpenetrating continuous phases and mass and momentum balances are solved for both fluids including their transfers at the interfaces. Turbulence can be described by different approaches, such as mixing-length models (Lance et al., 1996), two-equation models like the popular k-ε one (Laborde-Boudet et al., 2009), or Large Eddy Simulation (LES) models (Dhotre et al., 2009). In the last case, velocity fluctuations associated with large eddies are resolved while small scales are determined by appropriate Sub-Grid-Scale models. Literature abounds of works dealing with benefits and limits of every kind of turbulence models (Jakobsen et al., 2005).

When transport of chemical species is required in CFD simulations, an important issue concerns the contribution of velocity fluctuations that are not explicitly solved. The transport equation of the concentration describes only the contribution of the average velocity while the diffusivity induced by velocity fluctuations is taken into account through closure laws involving turbulence characteristics. Concerning single-phase flows, a simple solution consists in using a turbulent Schmidt number (Sc_t) to estimate the contribution of turbulence to the global diffusivity of passive scalars (Combest et al., 2011):

$$D_t = \nu_t / Sc_t \qquad (1)$$

The Sc_t approach is considered as classical and well validated. Different values of Sc_t in the range [0.7 – 1] may be preconized following the type of flow (Combest et al., 2011). In case of turbulent dispersed flows, scalar diffusion can result from turbulence induced by both velocity gradients and by the agitation generated by the bubbles. One first possibility is to include the effect of bubbles within a global turbulent diffusivity. As bubbles increase the local fluid agitation, the apparent Schmidt number may be lower than the value classically used for single-phase flows. Radl and Khinast (2010) report values between [0.4-0.7] depending on the turbulence model. This pragmatic approach can lead to satisfying results even if it is not based on a strong theoretical asset. It is however only appropriate

when shear-induced turbulence is largely dominant compared to BIT. Equation (1) obviously leads to a low diffusivity when turbulent viscosity tends towards zero although in such conditions bubble-induced turbulence still disperses passive scalars. Sato et al. (1981) propose an alternative approach by directly including the contribution of bubble wakes in the turbulent viscosity ν_t. This approach is however not able to deal with the decrease of ν_t caused by the presence of bubbles that is observed in some cases (Serizawa et al., 1992), and is therefore more suitable to flows governed by wall-induced turbulence. More recently, Ayed et al. (2007) also introduced a supplementary diffusivity due to bubble motions, which leads to an additional scalar diffusivity proportional to $\alpha_g d U_R$, in agreement with Sato et al. (1981).

Adding a specific diffusivity to account for the contribution of the bubbles to the mixing seems a more relevant approach referring to the experimental work of Alméras et al. (2014, 2015). This work has shown that the mixing induced by bubbles is well described by a regular diffusion process, the effective diffusion coefficients of which have been measured in vertical and horizontal directions for gas holdup from 1% to 13%. Following the Taylor's approach (Taylor, 1921), Alméras et al. propose to write the diffusivity coefficient $D_{i,i}$ as the product of the variance of the velocity fluctuations $u_i'^2$ by a diffusion timescale T_m ($D_{i,i} \propto u_i'^2\, T_m$). As described by Lance and Bataille (1991) or Riboux et al. (2010), the variance of the velocity fluctuations currently evolves as $u_i'^2 = \gamma_i^2 U_R^2 \alpha_g$. Concerning the diffusion timescale, two regimes of diffusion have been identified depending on the holdup. At low holdup, the diffusion timescale is evaluated as $T_m = \Lambda/u_i'$ (Corrsin, 1963), where Λ is the Eulerian integral length scale which does not depend on the holdup (Riboux et al., 2010). Consequently, at low holdup, the diffusivity coefficient evolves like $\alpha_g^{0,5}$ (Alméras et al, 2015). At large holdup, the diffusion timescale is limited by the average time interval between two bubbles passages, which is proportional to $d/(\alpha_g U_R)$. In this case, the diffusivity coefficient is proportional to $U_r d$ and independent of α. It is important to notice that due to the anisotropy of the velocity fluctuations, the mixing induced by bubbles is anisotropic whatever the diffusion regime. The diffusivity coefficient in the vertical direction is twice or even larger than that in the horizontal direction. Moreover, the transition between the two diffusion regimes occurs for a lower holdup in the horizontal direction than in the vertical one.

Based on the analysis of Alméras et al. (2015), the following model for the diffusion coefficients which accounts for the mixing by the BIT is proposed

$$D_{i,i} = \begin{cases} D_{i0}\alpha_g^{0,5} & \text{if } \alpha_g \le \alpha_{gc,i} \\ k\gamma_i^2 U_R d & \text{if } \alpha_g > \alpha_{gc,i} \end{cases} \qquad (2)$$

with the parameters reported in Table 1. Note that $D_{i0}=a_i U_R \Lambda$, where the prefactor a_i has been adjusted so that the diffusion coefficients in the vertical direction ($D_{x,x}$) and in the horizontal direction ($D_{y,y}$) are continuous at $\alpha_{gc,x}$ and $\alpha_{gc,y}$, respectively. It is also important to notice that this model differs from those of Sato et al. (1981) and Ayed et al. (2007) which introduce diffusion coefficients that are proportional to α_g.

To sum up, there are various possibilities to account for the effect of bubbles on scalar diffusivity. A simple adjustment of the turbulent Schmidt number is attractive for engineers but needs to be validated for each kind of application as it may hide more complex phenomena. On the other hand, recent developments concerning diffusion by B.I.T. such as the model described by eq. 2, are promising but

restricted to homogeneous bubbly flows. We now need to assess whether the diffusion by S.I.T. and by BIT can be added to address practical situations where both types of agitation are present.

In the present work, it is proposed to study bubbly flows in non-homogeneous conditions with the aim to test the validity of the model of Alméras et al. (2015). A 37L air/water bubble column is used with a gas injection that generates a flow recirculation. Low gas flow rates (V_{sg} < 1cm/s) are investigated in order to produce flows that are relatively easy to simulate with two-fluid models and where turbulence and bubble wakes may generate diffusivities of similar magnitudes. First, time experiments are performed by means of a colorimetric method. An in-house image processing is used to estimate mixing times. The method has been previously developed to measure mixing times in aerated stirred bioreactors (Gabelle et al., 2011). In a second step, hydrodynamics of investigated flows is modelled using a two-fluid CFD code. Once hydrodynamics is validated, simulations of tracer injections are performed in order to compare simulated overall mixing times to measured ones. Scalar mixing are simulated for different values of Sc_t, and with or without adding the diffusivity model of Alméras et al. (2015). Conclusions are drawn from comparisons between experiments and CFD simulations and recommendations are proposed concerning the modelling of scalar transport in bubbly flows.

2. Experimental setup and measurement method

A schematic of the experimental mock-up is shown in Fig.1. Experiments are carried out in a 300-mm diameter cylindrical glass column. The height of water is H=0.53m for each experiment. Concerning air injection, three types of distributor plates have been used. The first distributor (#1) is a plane plate of diameter 25cm, drilled of 35 holes equally spaced. The holes have a diameter of 1mm and follow a triangular step of 4cm. The second distributor (#2) is a modification of the first one, 31 holes have been clogged up using tape in order to allow air only through a central ring of 6 holes. The third one (#3) involves only 15 holes, all being located on the same half section of the whole distributor. Only the first distributor has been used for comparison with CFD. Fig.1 presents the complete distribution device. After 10 minutes of flow stabilization, 10mL of a dye tracer (Purple Drimarene R 2RL Clariant®) are injected by a device located at the centre of the column and at 9cm above the perforated bottom plate. The time of injection is approximately 2s. Immediately after each tracer injection, water is sent to rinse the injection pipe. This also shorten the effective time of injection. More details about the design of the injection device are given by Gabelle et al. (2011). Fig.2 illustrates the injection of dye and its mixing in the tank for the first and second gas distributors at different times after injection.

The global gas volume fraction α_g is measured by the elevation of the liquid level at the top of the column. The mean bubble size is measured by photography and semi-manual image treatment. The camera is also used to record the injection of dye and the mixing inside the tank. Mixing times are determined thanks to an in-house image processing software. Pictures are divided into several windows of 1 cm² and the mean grey level inside each window (maximum for lower concentrations and minimum for maximal concentrations) is computed and normalized by its final value so as to range between 0 and 1. The variance method described by Brown et al. (2004) is used to calculate mixing times:

$$log\sigma_{RMS}^2 = log\left\{\frac{1}{np}\sum_{i=1}^{np}(C_i - 1)^2\right\} \quad (3)$$

Where np is the number of probes and C_i the normalized signal of the probe i. Mixing is considered complete when $log\sigma^2_{RMS} = -2.6$, corresponding to an average standard deviation of 5% from the final concentration in the column. Mixing times have been measured inside the column for each distributor and for superficial gas velocities between 0.4 and 8mm/s, corresponding to gas flowrates between 0.1 to 2 m^3/h.

3. CFD modelling

2D axisymmetric transient simulations are performed using Fluent Ansys 14.5 CFD code. The choice of 2D simulations is legitimated by the work of Svendsen et al. (1992), who have experimentally observed that both gas and liquid flow patterns in a similar bubble columns are axisymmetric and that good agreements between experiments and axisymmetric simulations are often reached. As low gas velocities are involved, simulations converge to stationary flows, which justifies the use of 2D axisymmetric calculations. Simulations are carried out only in the configuration with the first gas distributor. The gas inlet is associated to an effective gas volume fraction $\alpha_G = 0.05$ and with a velocity that is adjusted to the targeted superficial gas velocity. The distributor with 35 holes is considered as an equivalent porous plate of 28cm of diameter. Walls are set with a no slip-condition and the top of the column to an atmospheric pressure outlet. A first order pressure-based solver is used with an implicit unsteady formulation. Gradients are estimated by a Green-Gauss cell based method. Then, momentum, volume fraction, turbulent kinetic energy and specific dissipation rate are solved using a First Order Upwind numerical scheme. Scalar concentration is solved using a Second Order Upwind numerical Scheme. The coupling between pressure and velocity is made with the SIMPLE algorithm.
Calculations are converged when all the normalized residues at each time step fall under 10^{-4} or when a maximum of 50 iterations per time step is achieved. The time step is set to 0.01s for all cases except for the smallest flow rate Q=0.1 m^3/h for which it is set to 0.001s in order to avoid the solver divergence. The mesh is composed of 0.002m side squares for a total number of 26250 cells. During the simulations, the tracer is introduced punctually using a cylindrical patch of 0.05m height and 0.05m diameter since the injection time of the tracer into the bubble column constitutes less than 10% of the mixing time for small flow rates. The standard deviation of the scalar concentration is used to calculate the mixing time during CFD simulations. This is equivalent to using eq. 3 with an infinite number of probes.

The numerical simulations are based on the two-fluid model with an Euler-Euler approach. The standard Euler-Euler equations for mass and momentum of phase k are written below:

$$\frac{\partial \alpha_k \rho_k}{\partial t} + \nabla.(\alpha_k \rho_k \boldsymbol{u}_k) = 0 \tag{4}$$

$$\frac{\partial}{\partial t}(\alpha_k \rho_k \boldsymbol{u}_k) + \nabla.(\alpha_k \rho_k \boldsymbol{u}_k \boldsymbol{u}_k) = -\alpha_k \nabla P + \alpha_k \rho_k \boldsymbol{g} \pm \boldsymbol{F}_{kl} + \nabla.(\alpha_k \boldsymbol{\tau}_k) + \nabla.\left(\alpha_k \rho_k \overline{\boldsymbol{u}'_k \boldsymbol{u}'_k}\right) \tag{5}$$

Where $\boldsymbol{F}_{kl}$ is the interfacial momentum exchange, $\overline{\boldsymbol{u}'_k \boldsymbol{u}'_k}$ the Reynolds stress tensor and $\boldsymbol{\tau}_k$ the viscous stress tensor expressed as:

$$\tau_k = \mu_{eff,k}\left(\nabla \boldsymbol{u}_k + \nabla \boldsymbol{u}_k^T - \frac{2}{3} I \nabla \boldsymbol{u}_k\right) \tag{6}$$

The $\boldsymbol{F}_{kl}$ term corresponds to the interaction forces between the phases. The predominant force to be considered in such system is the drag law (Svendsen et al., 1992 ; Laborde-Boutet et al., 2009. Other forces are neglected:

$$\boldsymbol{F}_{kl} = K_{kl}(\boldsymbol{u}_k - \boldsymbol{u}_l) \text{ with } K_{kl} = \frac{3\alpha_k\alpha_l}{4}\frac{\rho_l}{d_k}C_D|\boldsymbol{u}_k - \boldsymbol{u}_l| \quad (7)$$

The choice of the drag coefficient is discussed in part 4.1. RANS models are commonly used to simulate bubble columns (Jakobsen et al., 2005), and different approaches can be used to model the Reynolds stress tensor. In the present work, the turbulence k-ω model has been preferentially used as it is preconized in case of moderate Reynolds number. The transport equation solved for each scalar Φ_j into the liquid phase introduces an effective diffusion coefficient Γ_j.

$$\frac{\partial \rho_l \Phi_j}{\partial t} + \nabla.\left(\rho_l \boldsymbol{u}_l \Phi_j - \Gamma_j \nabla \Phi_j\right) = 0 \quad (8)$$

In the present work, the effective diffusion coefficient is modelled as the sum of two different contributions: the turbulent diffusion D_t and the bubble-induced diffusion$D_{i,i}$ given in eq. 2. The molecular diffusivity was neglected into the simulations.

$$\Gamma_{j,i} = \rho_l(D_t + D_{i,i}) \quad (9)$$

Implementation of the present model is realized through a routine involving eq. 1 and 2. A preliminary validation step has been conducted by simulating the dispersion of scalars in a stagnant flow for different values of the diffusivity coefficients$D_{i,i}$.

4. Results

The results are divided into two parts. Firstly, experimental and simulated hydrodynamics are considered. Second, the transport of scalars is introduced and experimental and numerical mixing times are compared and discussed. The three gas distributors are experimentally investigated but only the first one (#1 with 35 holes) is considered for CFD simulations (Taylor, 1921).

4.1 Hydrodynamics

Bubble diameter, terminal velocity and gas holdup are calculated during the experiments. Mean Sauter bubble diameter measured during experiments are presented in figure 3. For the 1st gas distributor (35 holes), the bubble size is almost constant. Consequently, in the simulation, the bubbles diameter is fixed to 5.6mm and a constant drag coefficient is chosen in order to obtain a bubble terminal velocity of 0.2m/s, consistent with the experiments. Gas holdup resulting from CFD simulations are compared to experiments in figure 4 and a good agreement is found.

As no direct measurements of the liquid profiles have been made, the axial velocity profiles resulting from the simulations are compared to correlations proposed by Linneweber (1981), Joshi (1983), Kawase and Moo-Young (1986) or Berneman (1989). Correlations depend on the liquid velocity at the center of the column, which value is taken to experiments. In figure 5, simulated liquid radial velocity profiles are compared to the calculated ones for Qg=0.5m^3/h at a height of 40 cm above the gas injection. Even though there is a scattering at wall, the overall liquid velocity profiles are fairly similar. As discussed earlier, the turbulent viscosity is an important parameter for the scalar transport.

Hence the volume averaged turbulent viscosity ν_t is compared to 3 existing correlations (Riquarts, 1981 ; Devanathan et al., 1990 ; Burns and Rice, 1997) for different gas flow rates. Results are reported in figure 6. Correlations are also scattered, but the CFD results are in the range of the correlations.

Simulations have also been performed with other turbulence models as k-ε and RNG k-ε. No significant effects on the gas holdup have been found, but variations of the mean turbulent viscosity of the order of +/- 15% have been observed. Following eq. 1, this may lead to proportional variations of the turbulent diffusivities if no additional dispersion phenomenon is considered. Finally, gas holdup calculations are validated, and liquid phase velocity and turbulent viscosity are in agreement with literature. Therefore simulated hydrodynamics is considered satisfactory for the present purpose.

4.2 Mixing times

Experimental mixing times measured with the 3 distributors are reported in figure 7. The 3 configurations lead to similar results. A slope as $1/\sqrt{\alpha_g}$ is observed for all the configurations. Lowest mixing times are reached with the largest gas distributor (#1). When mixing is driven by a diffusion D in a vessel of characteristic length L, the mixing time is given by $T_m \propto L^2/D$. A first simplistic analysis of this result leads to a global apparent diffusivity following $\propto \sqrt{\alpha_g}$ for all flow configurations. This dimensional analysis is coherent with the model of Alméras (eq. 2) as only gas volume fractions lower than $\alpha_{gc,i}$ are investigated in the present study. It could indicate that the turbulent contribution to scalar diffusion is moderate.
Concerning CFD simulations, two models of diffusivity are considered. The first one only involves a turbulent Schmidt number (eq. 1) while in the second one the specific contribution of the B.I.T. (eq. 2) is added to that of the S.I.T. (eq. 1). In both cases, the Sc_t number is swept in the range [0.005-1.5]. Snapshots of the scalar transport simulation are presented in figure 8 for Q_g=0.5m^3/h, with Sc_t=0.7 and including the model of Alméras et al. (2015), at different times (from 0 to 14 sec). The snapshots illustrate the transport of the scalar by the liquid recirculation and its dispersion inside the vessel due to the conjugated effect of Shear-Induced-Turbulence and Bubble-Induced-Turbulence. In figure 9, the influence of the Schmidt number on the resulting mixing times is presented for a gas flow rate of Q_g=0.5m^3/h. Without any other contribution than the turbulent viscosity, the Sc_t number has to be reduced to 0.1 to approach the experimental mixing time. On the other hand, adding the model of diffusivity induced by bubbles leads to common values of the Sc_t number for single-phase turbulence (~ 0.7 to 1) (Combest et al., 2011). These two main observations are still valid for every gas flow rates.
Figure 10 presents the simulated mixing time taking into account or not the specific diffusion induced by bubbles (B.I.T) for every considered gas flow rates and for various values of the Schmidt number. When only the turbulent diffusion is considered, the Schmidt number has to be lowered to 0.2 or even 0.1 to obtain mixing times in agreement with experiments. Furthermore the effective Schmidt number strongly depends on the operating conditions. However, considering a Sc_t number of 0.7 to 1 and adding the diffusivity induced by B.I.T. leads to an evolution of the mixing time in good agreement with the experiments for every gas flow rates without any parameters adjustment. In this last case, simulated mixing times are poorly sensitive to the Sc_t number, as long as it stays in the range [0.7-1], in agreement with figure 9 where a plateau is observed. For that reason, a choice of a Sc_t ~ 0.8-0.9 is suggested to offset uncertainty concerning turbulent viscosity.

5. Conclusions

In this work mixing of a passive scalar has been investigated experimentally and numerically in complex bubbly flows at moderate gas holdup ($\alpha_g \leq 3\%$). Experimental mixing times have been measured by an in-house image processing for three gas injection devices. An evolution of the mixing times following $1/\sqrt{\alpha_g}$ trends has been observed. The mixing experiments based on 35 holes for gas injection have been used as validation data for numerical modelling.

For this purpose, the commercial Eulerian RANS model implemented in Fluent has been used and 2D axisymmetric simulations have been performed. Hydrodynamics modelling has been validated first by comparing the simulated global gas volume fraction to experiments. Then, normalized liquid velocity profiles and turbulent viscosities have been compared to correlations. Mixing-time experiments have then been simulated by adding or not the contribution of B.I.T. modelled by Alméras et al. 2015. Various values of the turbulent Schmidt number from 0.1 to 1 have been tested too. A good agreement between experiments and modelling is reached with expected values of Sc_t number in the range of [0.7-1] only when the specific diffusivity induced by the bubbles is accounted for. If not, dramatically low values of Sc_t number have to be assigned to approach experimental mixing times.

As a conclusion, the comparison between experiments and CFD modelling shows that the B.I.T contribution to scalar diffusivity impacts strongly the mixing in the investigated flows, and has to be taken into account as an explicit contribution independent of the shear-induced turbulence to predict well the mixing of scalars.

Acknowledgements

The authors are grateful to Pierre Loup Buiret and Javier Rey Rueda for their active contributions to the experiments and simulations respectively.

Nomenclature

C_D	Drag law coefficient
C_i	Normalized concentration of tracer at probe i
d	Bubble diameter (m)
D	Isotropic diffusivity coefficient (m^2/s)
D_{i0}	Constant in eq. 2
$D_{i,i}$	Diffusion coefficient in direction i accounting for anisotropic diffusion by bubbles (m^2/s)
D_t	Diffusion coefficient accounting for isotropic diffusion by turbulence (m^2/s)
$\boldsymbol{F}_{kl}$	Interaction force between gas and liquid
$\boldsymbol{g}$	Gravity (m^2/s)
I	Identity matrix
k	Constant in eq. 2
K_{kl}	Momentum exchange coefficient
L	Characteristic length scale (m)
np	Number of probes
P	Pressure (Pa) in eq. 7
Q_g	Flow rate (m^3/h)
Sc_t	Turbulent Schmidt number
t	Time (s)
T_m	Characteristic time of the transport of scalar (s)
$\boldsymbol{u}_k$	Velocity vector of phase k (k=g for gas and k=l for liquid) (m/s)
$\boldsymbol{u'}_k$	Vector of velocity fluctuation of phase k, (m/s)
$\boldsymbol{u}_k^T$	Transposed vector of phase k velocity (m/s)
$u_i'^2$	Variance of the liquid velocity fluctuation in the direction i, (m^2/s^2)
U_R	Relative velocity between gas and liquid (m/s)
V_{sg}	Superficial gas velocity (m/s)
x_i	Direction i

Greek

$\alpha_{gc,i}$	Volume fraction threshold in direction i, in eq. 2
α_k	Volume fraction of phase k (k=g for gas and k=l for liquid)
α_l	Liquid volume fraction
γ_i	Standard deviation of average squared velocity fluctuations
$\Gamma_{j,i}$	Diffusion coefficient on direction i (m^2/s)
Λ	Integral of Lagrangian velocity fluctuations length scale
$\mu_{eff,k}$	Effective viscosity of phase k (k=g for gas and k=l for liquid) (kg/m.s)
ν_t	Turbulent kinematic viscosity (m^2/s)
ρ_k	Fluid density (k=g for gas and k=l for liquid) (kg/m^3)
σ_{RMS}	Standard deviation of tracer normalized concentration
τ_k	Viscous stress tensor
Φ_j	J^{th} scalar

References

Alméras, E, Risso, F., Roig V., Cazin S., Plais C., Augier F., 2015. Mixing by bubble-induced turbulence. Journal of Fluid Mechanics *under review*.

Alméras, E., 2014. Etude des propriétés de transport et de mélange dans les écoulements à bulles. Ph.D. thesis, Toulouse University.

Ayed, H., Chahed, J., Roig, V., 2007. Hydrodynamics and Mass Transfer in a Turbulent Buoyant Bubbly Shear Layer. AIChE Journal 53, 2742-2753.

Bernemann, K., 1989. Zur Fluiddynamik und zum Vermischungsverhalten der flüssigen Phase in Blasensäulen mit längsangeströmten Rohrbundeln. Ph.D. Thesis, University Dortmund.

Brown, A.R.D., Jones, P., Middleton, C.J., Papadopoulos, G., Arik, E.B., 2004. Experimental Methods, in L. E. Paul A. V. Atiemo-Obeng and M. S. Kresta, Eds., Handbook of Industrial Mixing, John Wiley & Sons, Inc., Hoboken, 145–256.

Burns, L.F., Rice, R.G., 1997. Circulation in bubble columns, AIChE Journal 43, 1390–1401.

Combest, D.P., Ramachandran, P.A., Dudukovic, M.P., 2011. On the gradient Diffusion Hypothesis and Passive Scalar Transport in Turbulent Flows. Industrial Engineering Chemistry Research 20, 8817-8823.

Corrsin, S., 1963. Estimates of the relation between eulerian and lagrangian scales in large reynolds number turbulence. Journal of Atmospheric Science 20, 115–119.

Dai, J., Sterling, J.D., Nadim, A., 2004. Numerical simulation of air bubbles rising in water using an axisymmetric VOF method. Computational Methods in Multiphase Flow II, Advances in Fluid Mechanics Series 37, 343-351.

Deckwer, W.D., 1992. Bubble Column Reactors.Wiley.

Delnoij, E., Kuipers, J.A.M.H., van Swaaij, W.P.N. 1997. Computational fluid dynamics applied to gas-liquid contactors. Chemical Engineering Science 52, 3623-3638.

Devanathan, N., Moslemian, D., Dudukovic, M.P., 1990. Flow mapping in bubble columns using CARPT. Chemical Engineering Science 45, 2285-2291.

Dhotre, M.T., Niceno, B., Smith, B.L., Simiano, M., 2009. Large-eddy simulation (LES) of the large scale bubble plume. Chemical Engineering Science 64, 2692-2704.

Gabelle, J.C., Augier F., Carvalho A., Rousset, R., Morchain J., 2011. Effect of Tank Size on kLa and Mixing Time in Aerated Stirred Reactors with Non-Newtonian Fluids. Canadian Journal of Chemical Engineering 89, 1139-1153.

Jakobsen, H.A., Lindborg, H. Dorao, C.A., 2005. Modeling of bubble column reactors: Progress and limitations, Industrial Engineering Chemistry Research 44, 5107-5151.

Joshi, J.B., 1983. Solid-liquid fluidised beds: some design aspects. Chemical Engineering Research and Design 61, 143-161.

Kawase, Y., Moo-Young, M., 1986. Liquid phase mixing in bubble columns with newtonian and non-newtonian fluids. Chemical Engineering Science 41, 1969-1977.

Laborde-Boutet, C., Larachi, F., Dromard, N., Delsart, O., Schweich, D., 2009. CFD simulation of bubble column flows: Investigations on turbulence models in RANS approach. Chemical Engineering Science 64, 4399-4413.

Lance, M., Bataille, J., 1991. Turbulence in the liquid phase of a uniform bubbly air-water flow, Journal of Fluid Mechanics 222, 95-118.

Lance, M., Tran M.L., Petersen K., 1996. Modelling of gas-liquid flow in bubble regime, Oil and Gas Science and technoloiges. Revue de l'Institut Français du Pétrole 51, 279-289.

Lau, Y.M., Bai, W., Deen, N.G., Kuipers, J.A.M.H., 2014. Numerical study of bubble break-up in bubbly flows using a deterministic Euler-Lagrange framework. Chemical Engineering Science 108, 9-22.

Laurent, A., Charpentier, J.C., 1974. Aires interfaciales et coefficients de transfert de matière dans les divers types d'absorbeurs et de réacteurs gaz-liquide. Chemical Engineering Journal 8, 85-101.

Li, Y., Zhang J.P., Fan, L.S., 2000. Discrete-phase simulation of single bubble rise behavior at elevated pressures in a bubble column. Chemical Engineering Science 55, 4597-4609.

Linneweber, K.W., 1981. Örtliche Gehalte an Gas sowie an Gas und Feststoff in Blasensäulen. Ph.D. Thesis, TU München.

Radl, S., Khinast, J.G., 2010. Multiphase Flow and Mixing in Dilute Bubble Swarms, AIChE Journal 56, 2421-2445.

Rafique, M., Chen, P., Dudukovic, M.P., 2004. Computational modeling of gas-liquid flow in bubble columns. Reviews in Chemical Engineering 20, 225-375.

Riboux, G., Risso, F., Legendre, D., 2010. Experimental characterization of the agitation generated by bubbles rising at high Reynolds number, Journal of Fluid Mechanics 643, 509-539.

Riquarts, H.P., 1981. A physical model for axial mixing of the liquid phase for heterogeneous flow regime in bubble columns. German Chemical Engineering 4, 18-23.

Sato, Y., Sadatomi, M., Sekogushi, K., 1981. Momentum and Heat Transfer in Two-Phase Bubble Flow-I. International Journal of Multiphase Flows 7, 167-177.

Serizawa, A., Kataoka I., Michiyoshi, I., 1992. Phase Distribution in Bubbly Flow. In: G.F. Hewitt, J.M. Delhaye, N. Zuber, Ed. Multiphase Science and Technology, 6, Washington DC: Hemishpere Publishing Corporation, 257-301.

Svendsen, H., Jakobsen, H., Torvik, R., 1992. Local flow structures in internal loop and bubble column reactors. Chemical Engineering Journal, 47, 3297-3304.

Taylor, G.I., 1921. Diffusion by continuous movements, Proceedings of The London Mathematical Society 2-20, 1, 196-212.

Table Captions
Table 1: Parameters of the diffusivity model of Alméras (2015).

Figure Captions

Figure 1: Schematic of the experimental setup: 300 mm diameter bubble column, air distributor and tracer injection. To the left: side view. To le right: top view of the air distributor.

Figure 2: Dye injection and mixing at different times. First row: distributor 1. Second row: distributor 2. From left to right: Q_g = 0.5 m^3/h. t=2s, 6s and ∞.

Figure 3: Bubble Sauter diameter versus superficial gas velocity (3 distributors).

Figure 4: Gas holdup: experiments (3 distributors) and CFD simulation (distributor 1).

Figure 5: Radial liquid velocity profile: CFD and Correlations.

Figure 6: Volume average turbulent viscosity: CFD and existing correlations versus Vsg.

Figure 7: Experimental mixing times for the 3 distributors. The 3 lines corresponds to $1/\sqrt{\alpha}$ slopes.

Figure 8: CFD snapshots during scalar mixing simulation with Sc_t=0.7 including the model of Alméras et al. (2015). Q_g = 0.5 m^3/h, t=0, 2, 4, 6, 8, 10, 12, 14s from left up to right down.

Figure 9: Mixing time from simulations at Q_g = 0.5 m^3/h and for various Sc_t numbers. Including or not the diffusivity model of Alméras et al. (2015).

Figure 10: Mixing time versus Vsg. CFD and Experimental results. Top: only considering a turbulent Schmidt number. Down: including both a turbulent Schmidt number and the diffusivity model of Alméras et al. (2015).

Table 1

$\alpha_{gc,x}$	$\alpha_{gc,y}$	D_{x0}(m^2/s)	D_{y0}(m^2/s)	γ_x	γ_y	k
0.041	0.027	0.0045	0.0029	0.18	0.13	25

Figure 1

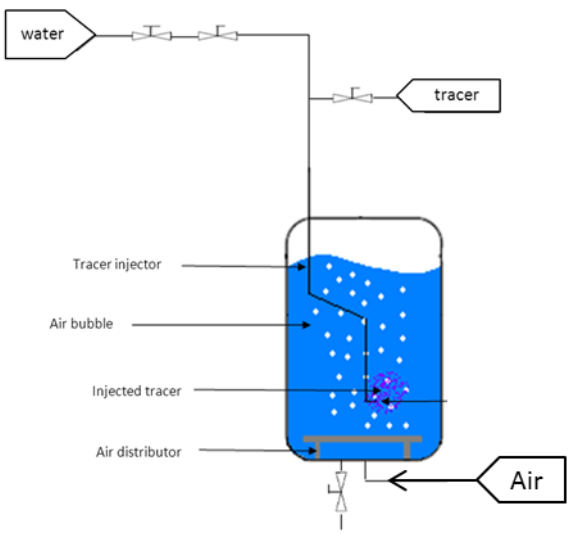
water
tracer
Tracer injector
Air bubble
Injected tracer
Air distributor
Air

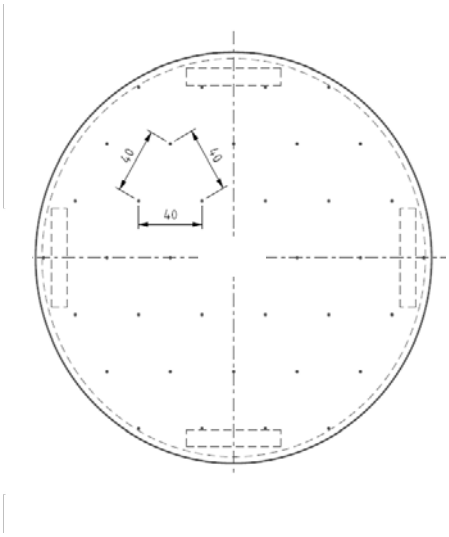
40
40
40

Figure 2

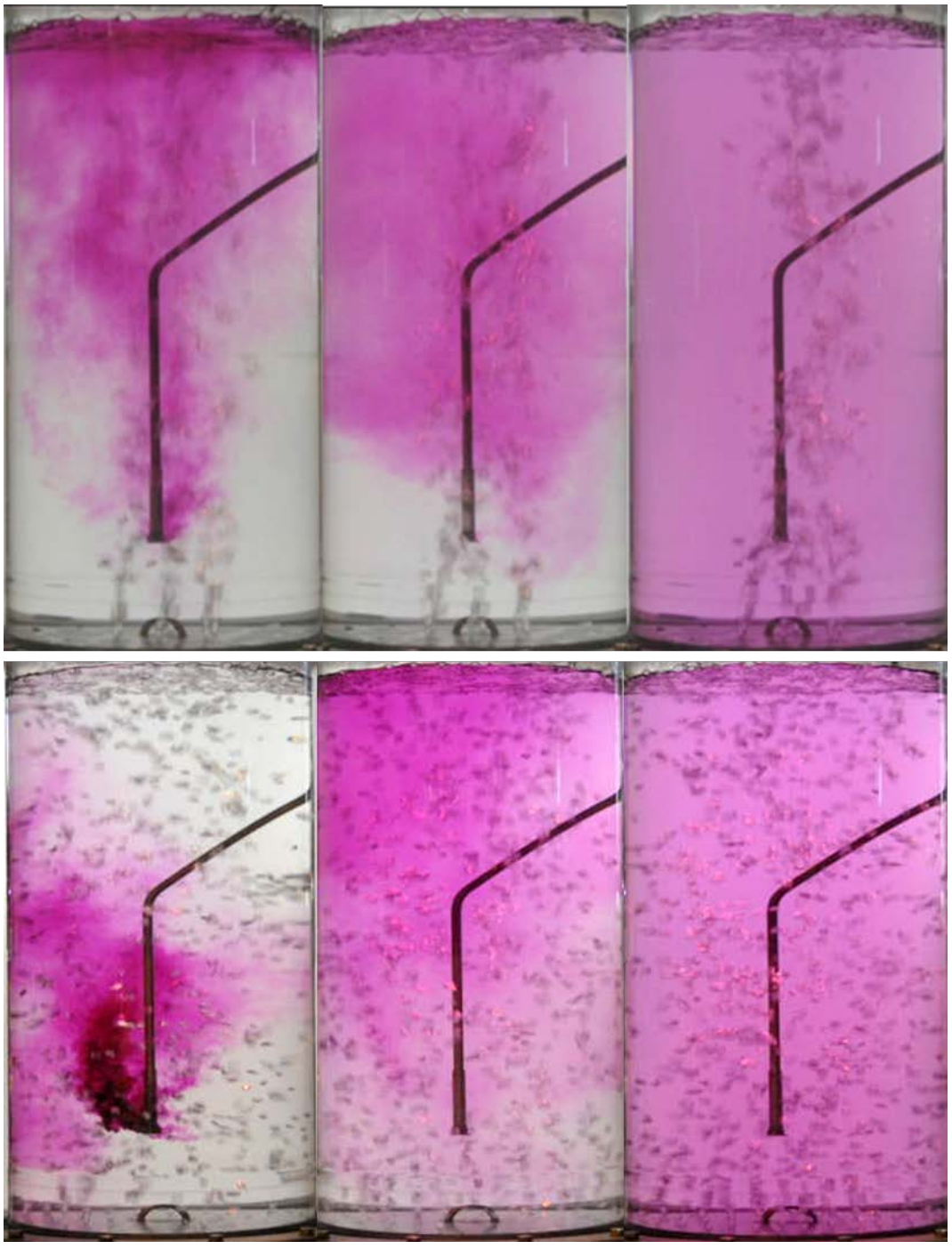

Figure 3

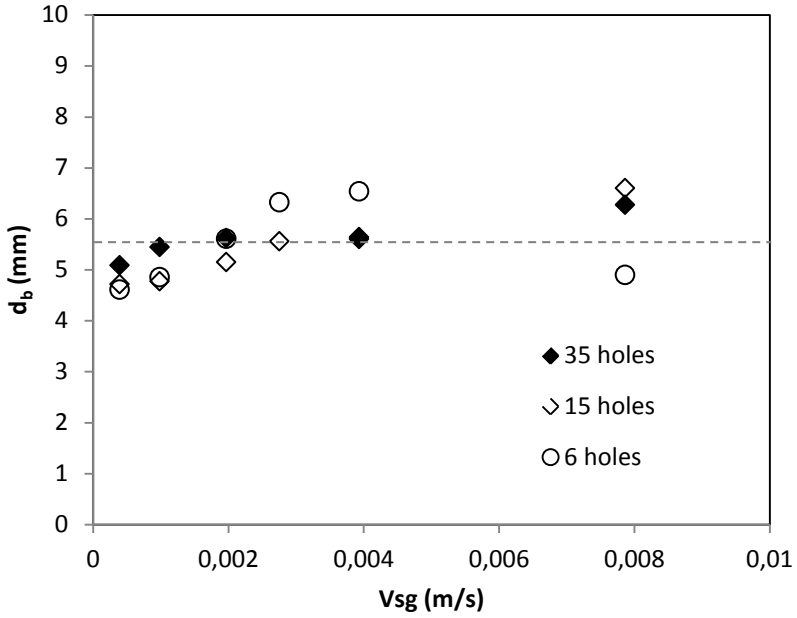
10
9
8
7
6
5
4
3
2
1
0
d_b (mm)
0
0,002
0,004
0,006
0,008
0,01
Vsg (m/s)
35 holes
15 holes
6 holes

Figure 4

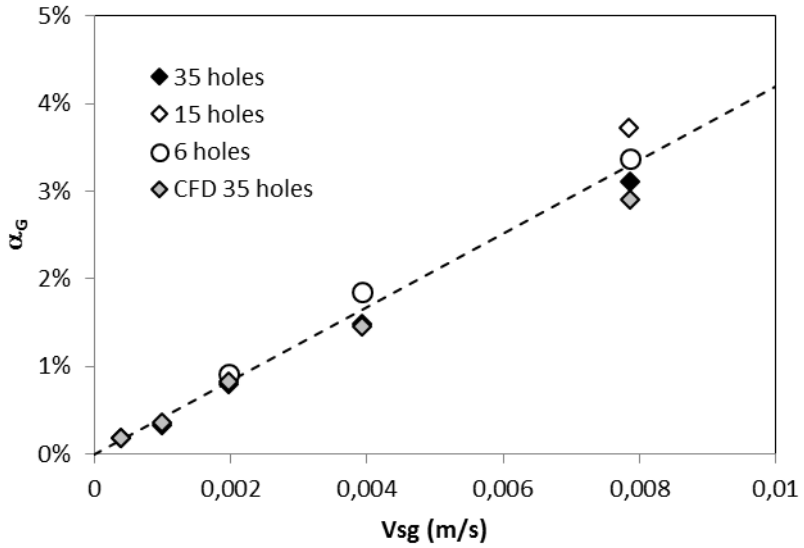
5%
4%
3%
2%
1%
0%
α_G
35 holes
15 holes
6 holes
CFD 35 holes
0
0,002
0,004
0,006
0,008
0,01
Vsg (m/s)

Figure 5

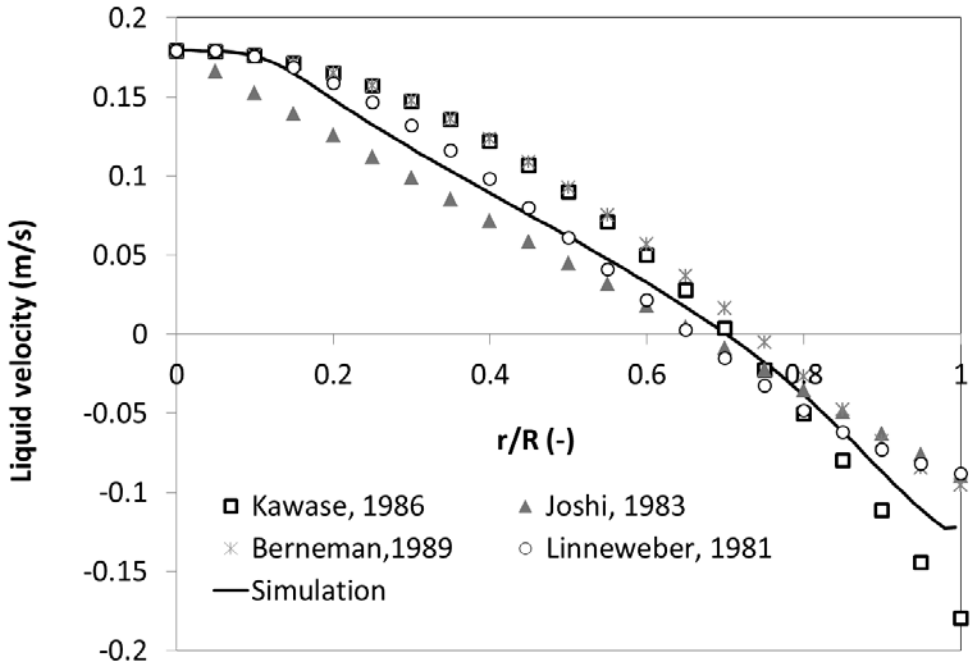
Liquid velocity (m/s)
0.2
0.15
0.1
0.05
0
-0.05
-0.1
-0.15
-0.2
0
0.2
0.4
0.6
0.8
1
r/R (-)
Kawase, 1986
Joshi, 1983
Berneman,1989
Linneweber, 1981
Simulation

Figure 6

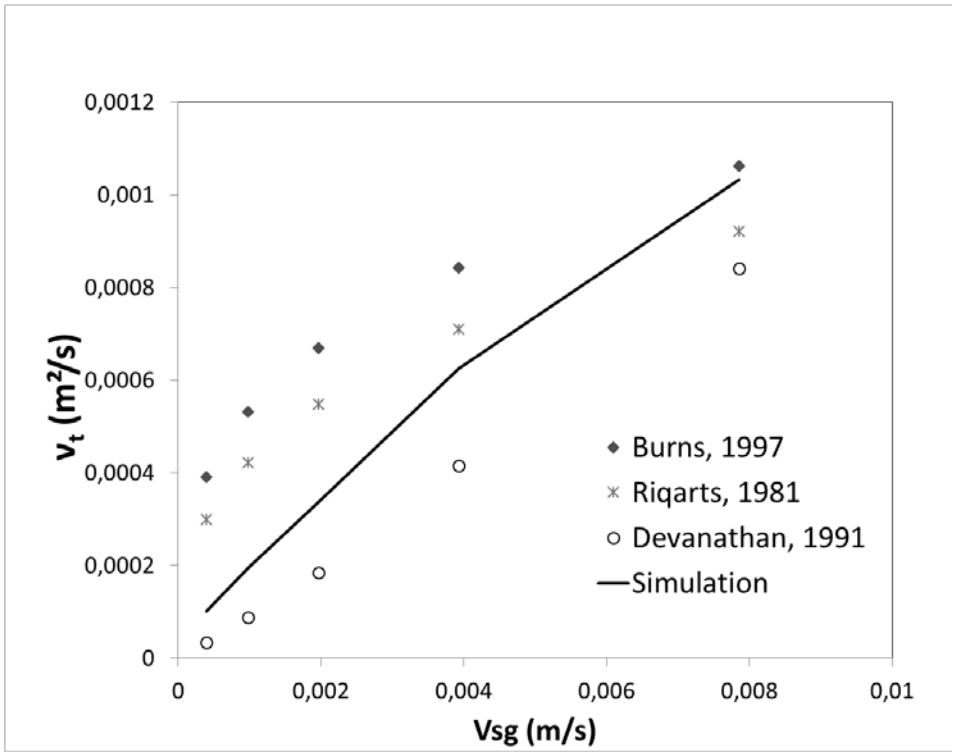
0,0012
0,001
0,0008
0,0006
0,0004
0,0002
0
v_t (m²/s)
0
0,002
0,004
0,006
0,008
0,01
Vsg (m/s)
Burns, 1997
Riqarts, 1981
Devanathan, 1991
Simulation

Figure 7

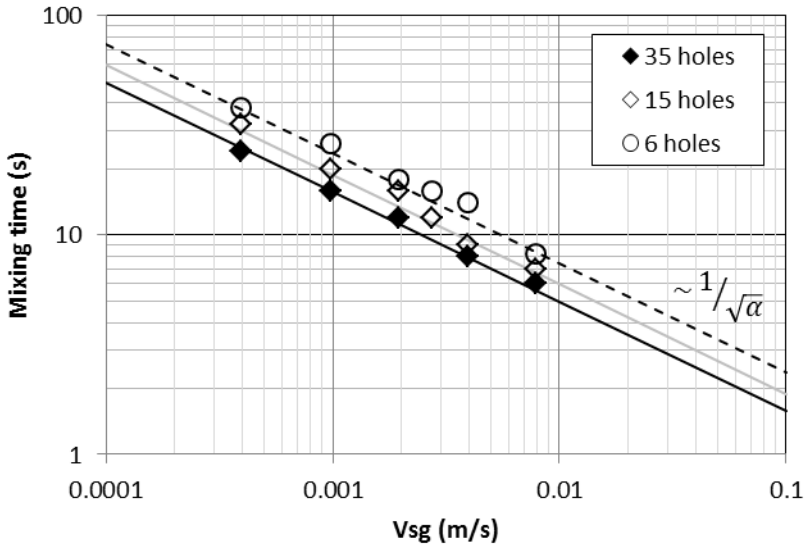
100
10
1
Mixing time (s)
0.0001
0.001
0.01
0.1
Vsg (m/s)
35 holes
15 holes
6 holes
$\sim 1/\sqrt{\alpha}$

Figure 8

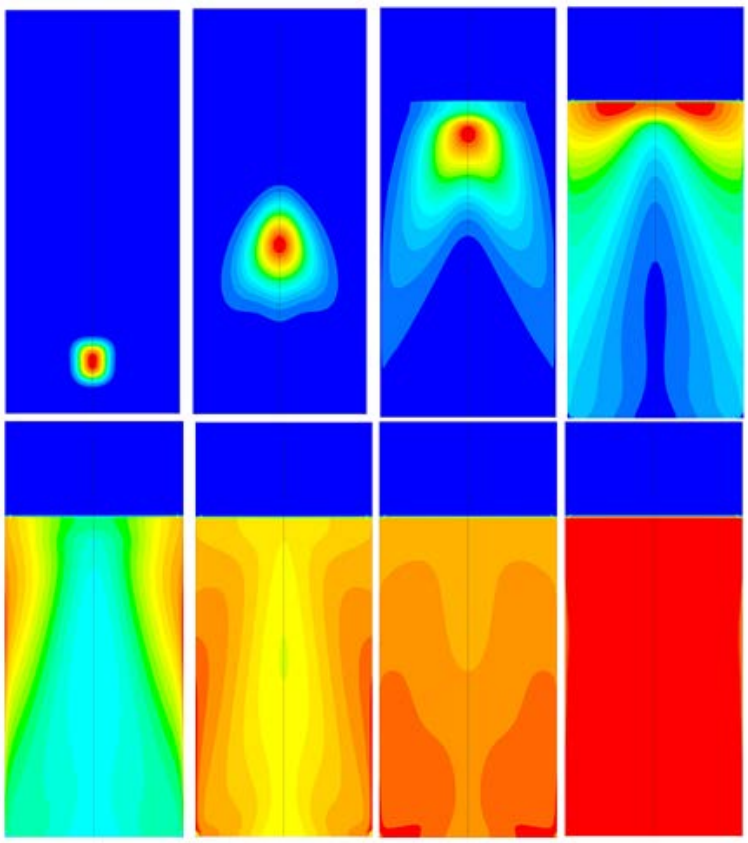

Figure 9

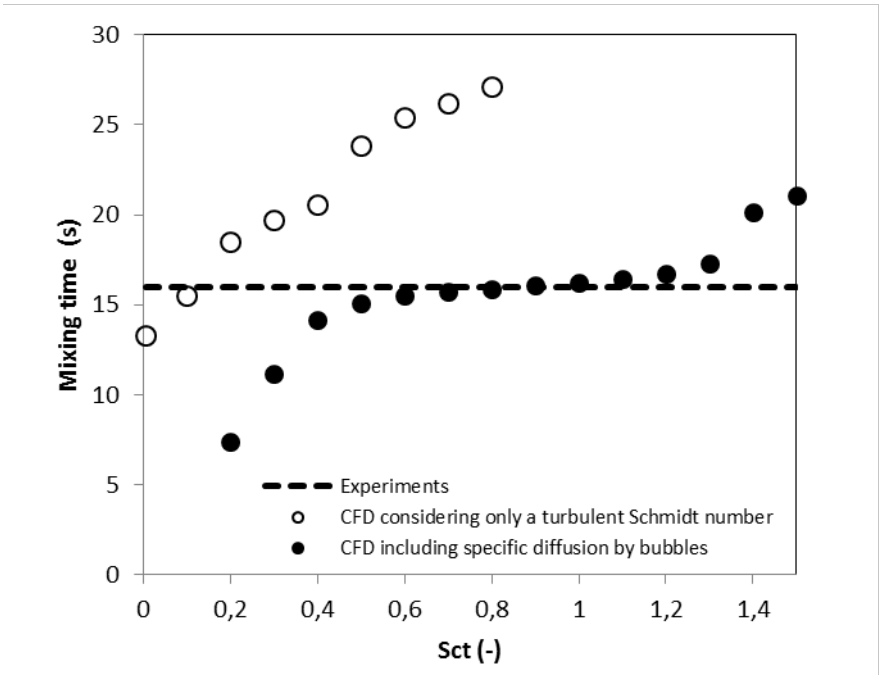
Mixing time (s)
30
25
20
15
10
5
0
0
0,2
0,4
0,6
0,8
1
1,2
1,4
Sct (-)
Experiments
CFD considering only a turbulent Schmidt number
CFD including specific diffusion by bubbles

Figure 10

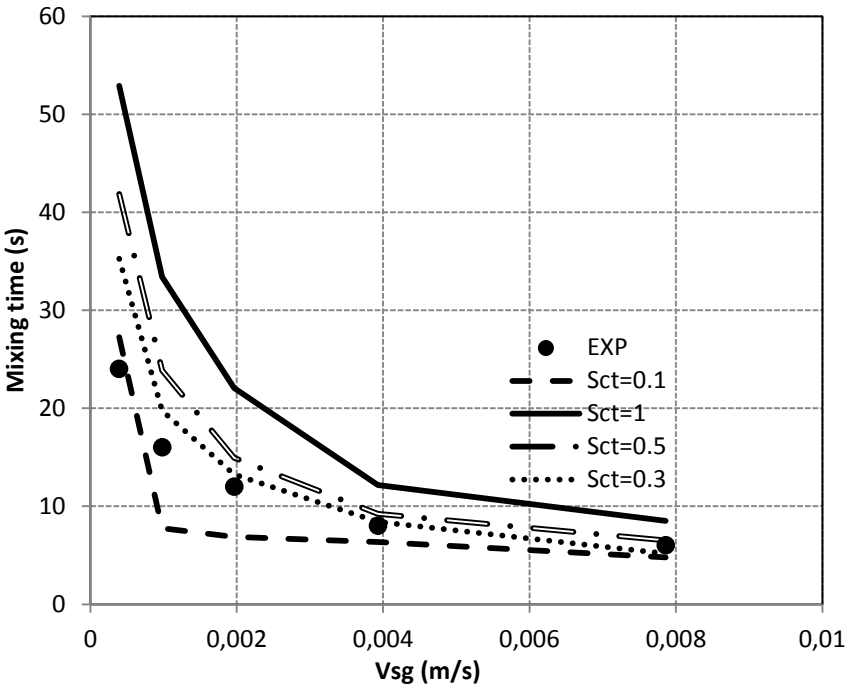
60
50
40
30
20
10
0
Mixing time (s)
0
0,002
0,004
0,006
0,008
0,01
Vsg (m/s)
EXP
Sct=0.1
Sct=1
Sct=0.5
Sct=0.3

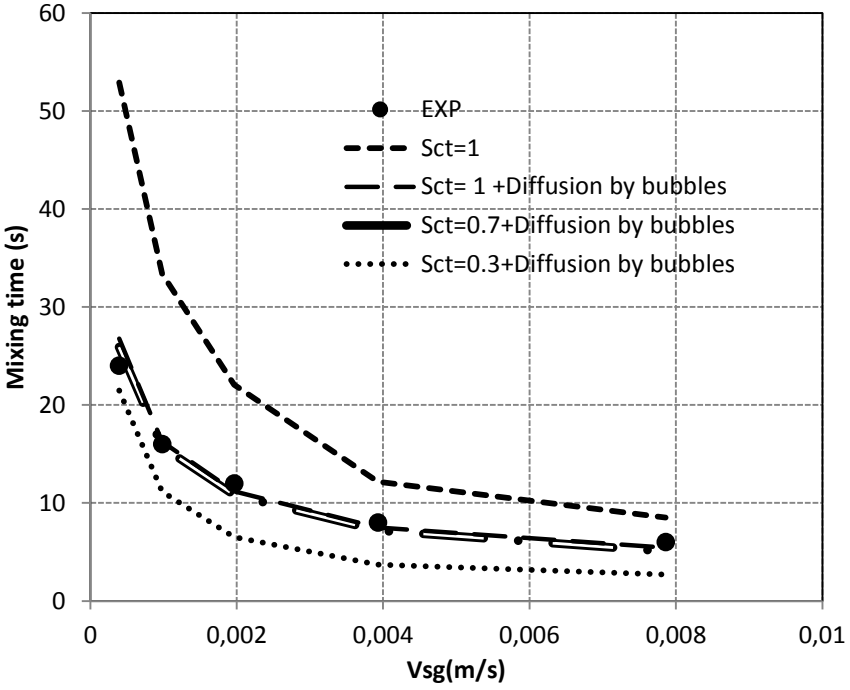
60
50
40
30
20
10
0
Mixing time (s)
0
0,002
0,004
0,006
0,008
0,01
Vsg(m/s)
EXP
Sct=1
Sct= 1 +Diffusion by bubbles
Sct=0.7+Diffusion by bubbles
Sct=0.3+Diffusion by bubbles